

# Continuous Large Area Monolayered Molybdenum Disulfide Growth Using Atmospheric Pressure Chemical Vapor Deposition

Rakesh K. Prasad and Dilip K. Singh\*

Cite This: *ACS Omega* 2023, 8, 10930–10940

Read Online

ACCESS |



Metrics &amp; More

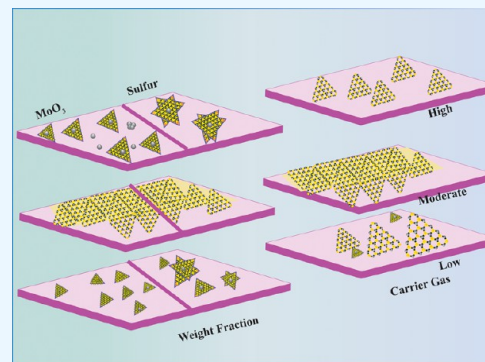


Article Recommendations



Supporting Information

**ABSTRACT:** The growth of large crystallite continuous monolayer materials like molybdenum disulfide ( $\text{MoS}_2$ ) with the desired morphology via chemical vapor deposition (CVD) remains a challenge. In CVD, the complex interplay of various factors like growth temperatures, precursors, and nature of the substrate decides the crystallinity, crystallite size, and coverage area of the grown  $\text{MoS}_2$  monolayer. In the present work, we report about the role of weight fraction of molybdenum trioxide ( $\text{MoO}_3$ ), sulfur, and carrier gas flow rate toward nucleation and monolayer growth. The concentration of  $\text{MoO}_3$  weight fraction has been found to govern the self-seeding process and decides the density of nucleation sites affecting the morphology and coverage area. A carrier gas flow of 100 sccm argon results in large crystallite continuous films with a lower coverage area (70%), while a flow rate of 150 sccm results in 92% coverage area with a reduced crystallite size. Through a systematic variation of experimental parameters, we have established the recipe for the growth of large crystallite atomically thin  $\text{MoS}_2$  suitable for optoelectronic devices.



## 1. INTRODUCTION

For nearly the past decade, two-dimensional (2D) semiconducting transition-metal dichalcogenides (TMDs),  $\text{MX}_2$  ( $\text{M} = \text{Mo}, \text{W}$ ;  $\text{X} = \text{S}, \text{Se}$ ) have attracted huge attention due to their distinct structural, physical, and chemical properties arising from the layered structure with van der Waals forces of interactions in between the layers opening up new possibilities in the form of efficient and thin electronic and optoelectronic devices.<sup>1–3</sup> Molybdenum disulfide ( $\text{MoS}_2$ ) is a layered 2D semiconducting material with a band gap in the range of 1.2–1.9 eV, whose optical and electrical properties are dependent on the number of layers.<sup>4</sup> Monolayered  $\text{MoS}_2$  is an atomically thin direct-band gap semiconductor with considerable enhancement in photoluminescence, while an increase in the number of layers shows indirect band gap semiconducting behavior.<sup>5</sup> Monolayered  $\text{MoS}_2$  have high potential applications in the domain of optoelectronics, nanoelectronics, and photonics.<sup>1,4</sup>

A number of techniques have been attempted to achieve large crystals of single-layered  $\text{MoS}_2$ . Initially, various types of exfoliation techniques were explored like scotch tape-assisted micromechanical exfoliation,<sup>6</sup> liquid-phase exfoliation,<sup>7</sup> and electrochemical Li-intercalation from bulk natural crystals.<sup>8</sup> These methods allowed one to achieve nanometer to few micrometer sizes of monolayered  $\text{MoS}_2$ . To grow films at the desired locations with the predefined number of layers having a large coverage area, different growth techniques were attempted like thermolysis of ammonium thiomolybdate,<sup>9</sup> physical vapor deposition,<sup>10</sup> atomic layer deposition,<sup>11,12</sup> hydrothermal synthesis<sup>13</sup> sulfurization of molybdenum

or molybdenum oxide film,<sup>17</sup> and chemical vapor deposition (CVD).<sup>14</sup> CVD-based growth has the potential to be integrated with in-line fabrication at foundries, making it the most favorable technique used for the synthesis of monolayered  $\text{MoS}_2$  having large crystallite sizes and continuity over a large area.

To elucidate the growth mechanism of  $\text{MoS}_2$  films using CVD, recently a number of experiments have been reported. One of the earlier attempts in 2012 used a pre-deposited Mo film followed by CVD-based sulfurization to achieve single and few-layered  $\text{MoS}_2$  on the Si/ $\text{SiO}_2$  substrate.<sup>14</sup> In 2014, using atmospheric pressure CVD and precursors in the form of sulfur and  $\text{MoO}_3$  powders, Wang et al. demonstrated that the local change of Mo/S precursor ratios govern the variation of the shapes of the crystals grown from triangular to hexagonal.<sup>18</sup> Growth of  $\text{MoS}_2$  films using  $\text{MoO}_3$  as a precursor shows triangular crystals, while  $\text{MoCl}_5$ -based growth results in continuous growth.<sup>19</sup> Single crystalline  $\text{MoS}_2$  flakes with a size larger than 300  $\mu\text{m}$  were grown by suppressing the nuclei density through adjusting the distance between sources and the substrate.<sup>20</sup> Single-step synthesis of monolayered large-area  $\text{MoS}_2$  films were performed on a variety of substrates by using

Received: November 18, 2022

Accepted: January 6, 2023

Published: March 15, 2023



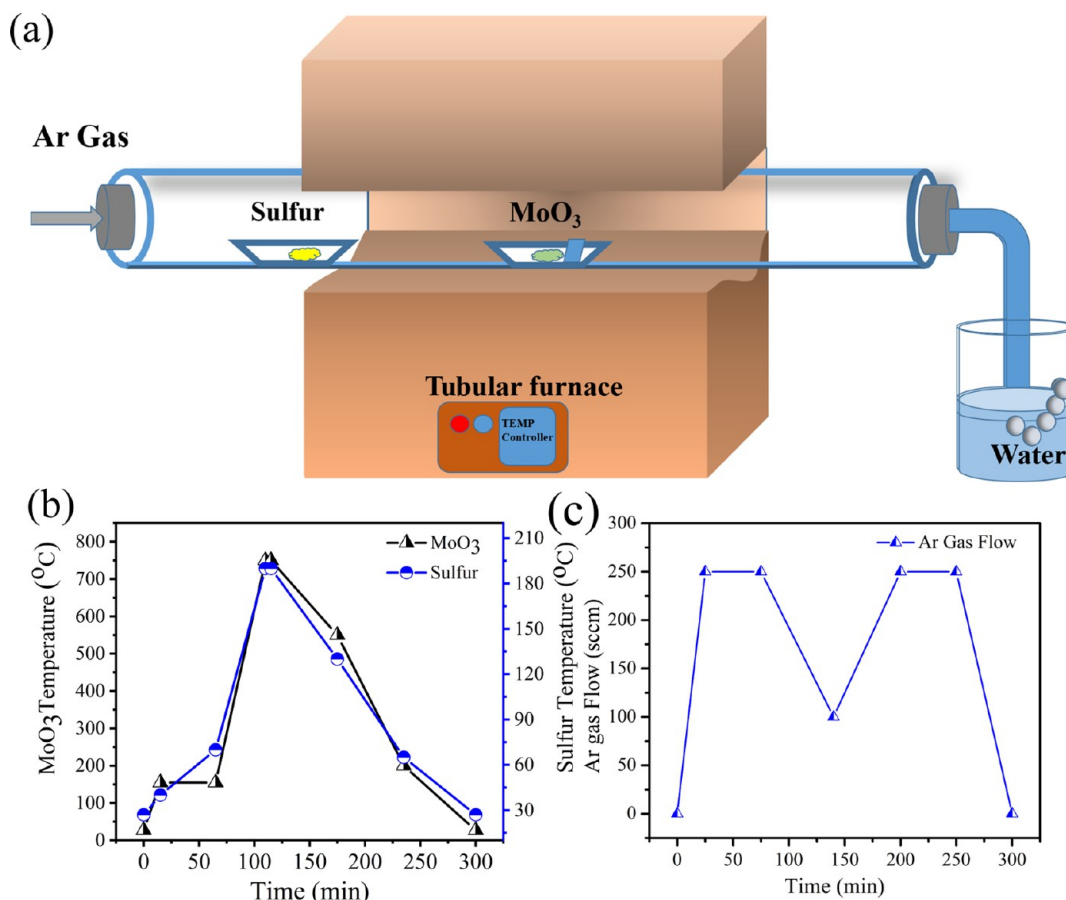


**Figure 1.** (a) Schematic setup for thermal CVD-based synthesis of MoS<sub>2</sub> monolayers and (b) temperature variation for MoO<sub>3</sub> and sulfur during the MoS<sub>2</sub> growth process. (c) Variation of gas flow rate during growth.

the naturally formed gap between SiO<sub>2</sub>-coated (285 nm)/Si-wafer and the substrate acting as reactor cavity.<sup>21</sup> In another experiment, MoO<sub>2</sub> was used as a precursor and growth kinetics of MoS<sub>2</sub> was elucidated. They observed the formation of two types of seeding centers: (a) Mo-oxysulfide (MoO<sub>x</sub>S<sub>2-y</sub>,  $y \geq x$ ) nanoparticles resulting in triangular growth for few layers MoS<sub>2</sub> and (b) atomic scale MoS<sub>2</sub> monolayer clusters to grow monolayers and an irregular polygon shape.<sup>22</sup> Zhou et al.<sup>23</sup> observed that the monolayered MoS<sub>2</sub> grown from irregular polygonal-shaped cluster decorated with S–Mo and Mo–zz edges in a comparable ratio with dominant Mo–zz edge formation grows. Reactant concentrations have been found to facilitate a 2D-planar nucleation mechanism responsible for monolayer/bi-layer growth, while higher concentrations lead to the self-seeding nucleation mechanism responsible for few-layered/multi-layered growth.<sup>23</sup> A comparison of growth quality using three different precursors, namely, MoO<sub>3</sub>, ammonium heptamolybdate, and tellurium (Te) assistance using MoO<sub>3</sub> for large continuous films using CVD shows better quality of large size growth using only MoO<sub>3</sub> powder and sulfur powder with a particular ratio of approximately 30:1.<sup>24</sup> Growth at varying temperatures shows that MoS<sub>2</sub> tend to grow laterally in triangular shapes at temperatures below 730 °C, while growth above 730 °C results in longitudinal growth with hexagonal shapes.<sup>25</sup> In spite of a number of notable attempts, a standard recipe for the growth of continuous large crystallites of MoS<sub>2</sub> remains a challenge.<sup>26,27</sup> A proper understanding of the growth mechanism is desirable for the CVD-based process to achieve a large crystallite continuous

monolayered film of MoS<sub>2</sub> having few grain boundaries which limits the mobility of the charge carriers.<sup>28</sup> During CVD-based growth of MoS<sub>2</sub>, a number of parameters like nature of the precursor used,<sup>29,30</sup> orientation of the substrate,<sup>31</sup> gas flow rate,<sup>23</sup> growth temperature and duration,<sup>25</sup> and use of promoters<sup>32</sup> are expected to affect the crystallite size, phase, and shape.

In this work, MoS<sub>2</sub> grown at various experimental conditions has been systematically investigated using spectroscopic tools to establish the recipe for the growth of continuous monolayered MoS<sub>2</sub> films having limited grain boundaries. The role of precursors and carrier gas on the grain boundary formation and triangular domains has been elucidated to achieve large-area MoS<sub>2</sub> atomically thin films for electronic and opto-electronic applications.

## 2. EXPERIMENTAL DETAILS

For MoS<sub>2</sub> growth, highly pure molybdenum trioxide MoO<sub>3</sub> (99.9% Sigma-Aldrich) and sulfur powder (99.9% Sigma-Aldrich) were used as precursors. Figure 1a shows the schematic of the CVD setup and the growth parameters are shown in Figure 1b,c. In CVD, a quartz tube of length of 120 cm and diameter of 4.5 cm was used. The temperature profile of both the precursors (MoO<sub>3</sub> and S powder) during the complete cycle of growth has been shown in Figure 1b, and gas flow rate for the complete experimental duration of 285 nm SiO<sub>2</sub>/Si wafer was used as a substrate for growth. The substrate was first cleaned sequentially using the iso-propyl alcohol, deionized water, and ethanol through a sonication bath process

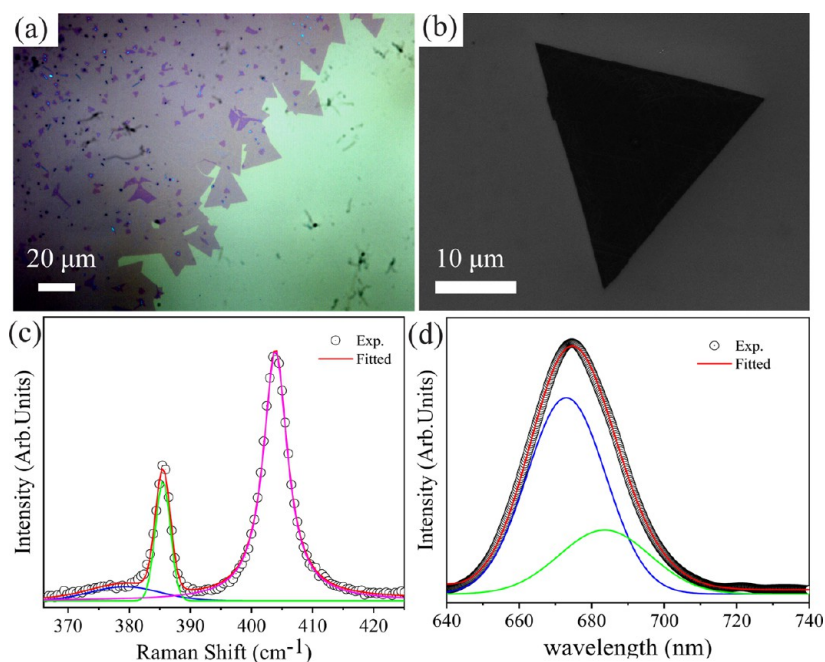


**Figure 2.** (a) Optical microscopy image of grown MoS<sub>2</sub> flakes, (b) field-emission electron microscopy (FESEM) images of MoS<sub>2</sub> grown on 285 nm—SiO<sub>2</sub>/Si, (c) Raman spectra of MoS<sub>2</sub>, and (d) photoluminescence spectra from grown MoS<sub>2</sub> films.

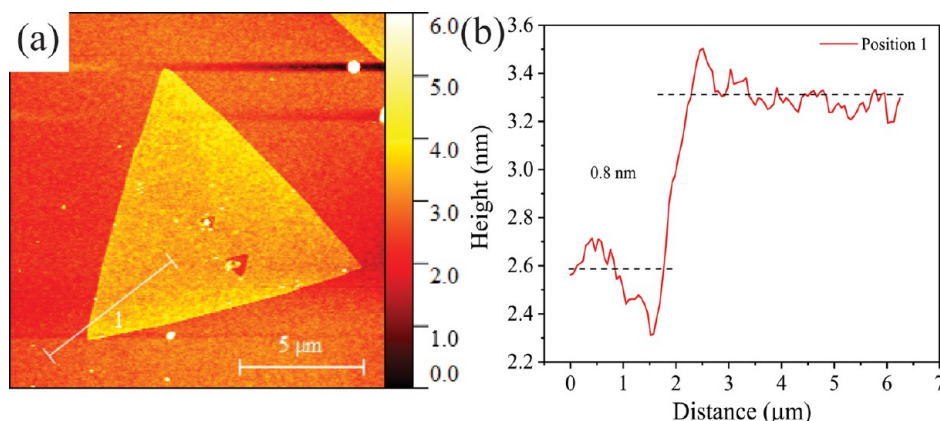


**Figure 3.** (a) AFM image of grown sample of MoS<sub>2</sub> (b) thickness profile of monolayer MoS<sub>2</sub>.

for 15 min each. After sonication, the substrate was washed with deionized water and then dried using the argon gas and put inside a hot oven at 100 °C for 10 min. The polished surface of the substrate faces downward to the precursor above the MoO<sub>3</sub> powder. Precursors and substrates were placed inside the CVD furnace, as schematically shown in Figure 1a, separated at 19 cm. The growth was carried out at 750 °C for 5 min using a single zone CVD furnace at atmospheric pressure. The outlet of the quartz tube was bubbled through a water bucket ensuring equilibrium argon pressure inside the tube. During growth, the amount of MoO<sub>3</sub> was varied between 10 and 30 mg and referred to as SET-I keeping the gas flow rate constant at 100 sccm and weight of sulfur 200 mg. In SET-II, the weight of the second precursor sulfur was varied in the range 100–500 mg keeping other conditions like weight of MoO<sub>3</sub> (15 mg) and gas flow rate (100 sccm) fixed. Finally, the carrier gas flow rate (argon) was varied in the range of 50–300 sccm referred to as SET-III, while keeping the other two factors MoO<sub>3</sub> and sulfur fixed at 15 and 200 mg, respectively.

### 3. CHARACTERIZATION

The growth of MoS<sub>2</sub> flakes was confirmed initially using an optical microscope (Leica) with a 10× (NA 1.3), 50× objective lens. The detailed morphology of grown samples was recorded using a field-emission electron microscope (ZEISS Sigma 300 FESEM). The number of layers of MoS<sub>2</sub> was characterized using a Raman spectrometer (LabRam HR800, Jobin-Yvon) in the range 350–450 nm. Photoluminescence spectra of samples were recorded in the range 640–740 nm using  $\lambda_{\text{ex}} = 532$  nm (laser excitation). The thickness and surface topography was measured by atomic force microscopy (AFM) (Cypher, Oxford Instruments) in a noncontact mode.

### 4. RESULTS AND DISCUSSION

Figure 2a shows the optical microscopy image of the grown continuous film of MoS<sub>2</sub> sample. Figure 2b shows the FESEM image of individual triangles at higher magnification from the grown continuous sheet of MoS<sub>2</sub> film. Raman spectra show two vibration modes at 385.7 (E<sub>2g</sub><sup>1</sup>) and 403.8 cm<sup>−1</sup>(A<sub>1g</sub>), as



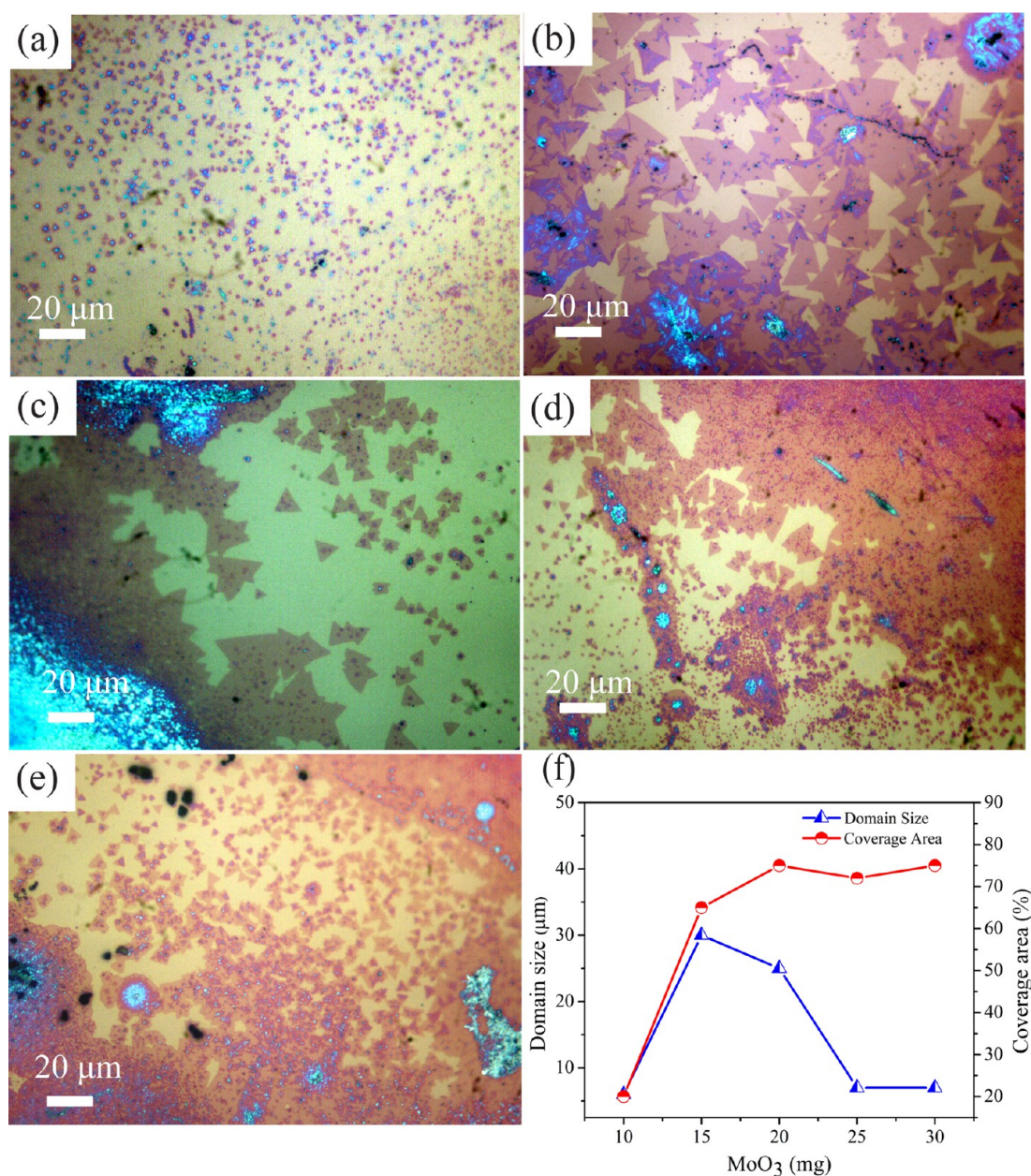


**Figure 4.** Optical micrographs of CVD-grown MoS<sub>2</sub> flakes with varying amounts of MoO<sub>3</sub> precursors (a) 10, (b) 15, (c) 20 (d) 25, (e) 30 mg, and (f) variation of domain size and coverage area with increasing weight of MoO<sub>3</sub>.

shown in Figure 2c. An observed frequency difference of 18.1 cm<sup>-1</sup> confirms the growth of monolayer MoS<sub>2</sub> in agreement with previous works.<sup>14,24</sup> The frequency difference between these two modes depends upon the number of layers.<sup>33</sup> Both the in-plane vibrational mode ( $E_{2g}^1$ ) and out-of-plane ( $A_{1g}$ ) modes show the requirement of two-peak structure for fitting the experimental curve, as shown in Figure 2c. A fitted line profile is summarized in Table S1 (see the Supporting Information). Interestingly, the in-plane vibrational mode ( $E_{2g}^1$ ) mode is Gaussian, while the out-of-plane ( $A_{1g}$ ) mode is Lorentzian in line-shape. Such two peak structures/splittings of in-plane vibrational mode ( $E_{2g}^1$ ) were previously observed in MoS<sub>2</sub> with a lattice strain of more than 1%, which arises due to the disorder in the crystalline structure of the material.<sup>34</sup> The photoluminescence spectra recorded from the same position is shown in Figure 2d. The experimental curve was fitted using the Gaussian line shape, which shows an emission peak at

673.0 nm (1.84 eV) with shoulders at 684.2 nm (1.81 eV) with relative intensities of 284.2 counts and 98.1 counts, respectively. The 1.84 eV peak is assigned to the A-exciton, while the 1.81 eV peak arises due to A<sup>-</sup> excitons.<sup>35,36</sup> A-exciton shows peak width  $\Delta\omega = 44.1$  nm, while the A<sup>-</sup> exciton shows  $\Delta\omega = 63.7$  nm. The observed strong A-exciton peak relative to the A<sup>-</sup> exciton indicates monolayer growth<sup>5</sup> in agreement with Raman spectra shown previously. Coehoorn et al. observed two prominent peaks at 670 and 627 nm in the absorption spectrum. These two resonances have been established to be the direct excitonic transitions at the Brillouin zone K-point. Their energy difference is due to the spin-orbital splitting of the valence band.<sup>35</sup> Figure 3a,b shows the AFM measurement of the sample grown using 15 mg of MoO<sub>3</sub> and 200 mg of sulfur under 100 sccm of argon flow. It shows a thickness of ~0.8 nm. The observed thickness is in the range of single-layer

MoS<sub>2</sub> thickness observed by others on the bare substrates (0.6–0.9 nm).<sup>33</sup>

Figure 4 shows the effect of MoO<sub>3</sub> weight fraction during growth. Figure 4a shows nucleation of small equilateral triangular domains grown randomly on the substrate having a crystallite size of  $\sim 7\ \mu\text{m}$  when 10 mg of MoO<sub>3</sub> was used along with 200 mg of sulfur. Lower concentrations of MoO<sub>3</sub> result in a lower growth rate. An optical image of growth with 15 mg MoO<sub>3</sub> indicates the formation of continuous films with a large crystal size of  $\sim 30\ \mu\text{m}$ . Increased MoO<sub>3-x</sub> vapor flux with increasing weight fraction of MoO<sub>3</sub> leads to increased growth rate resulting in the formation of continuous films with grain boundaries, as visible in Figure 4b. Grain boundaries of continuous film formation were observed due to a low mass flux and high growth rate.<sup>37</sup> Coalescence of the particles takes place resulting in the formation of continuous sheets with increased MoO<sub>3</sub> weight fraction to minimize the surface energy through reduction of the surface area. With further increase of MoO<sub>3</sub> concentration to 20 mg, multi-nucleation sites were observed under an optical microscope, as shown in Figure 4c. In this case, we observe a continuous film with a discrete crystal size range from  $\sim 7$  to  $25\ \mu\text{m}$  (Figure 4c). For 25 mg of MoO<sub>3</sub>, the crystal shape changes from sharp edged triangles to triangles with rounded corners having a crystallite size of  $7\ \mu\text{m}$ , as shown in Figure 4d. Further increase of MoO<sub>3</sub> weight fraction to 30 mg results in triangular crystals with a smaller size of  $\sim 7\ \mu\text{m}$  and higher nucleation density on the substrates, as shown in Figure 4e. Growth with increasing weight of MoO<sub>3</sub> relative to sulfur results in large crystals of MoS<sub>2</sub> flakes with continuous films tuned by the vapor phase of MoO<sub>3-x</sub>. The precursor evaporates in the form of flux, resulting in different size nanostructures. The deposition of MoO<sub>3-x</sub> molecular clusters are reduced to MoS<sub>2-x</sub> clusters (bright spots inside the triangle) in the initial stage of the growth process, consequently leading to a 2-dimensional nucleation on the SiO<sub>2</sub>/Si substrate (as shown schematically in Figure S1—Supporting Information).<sup>38</sup> The growth of MoS<sub>2</sub> is limited by the diffusion of vapor-phase MoO<sub>3-x</sub>.<sup>39</sup> Tuning of the weight fraction of precursors also affects the Mo/S molar ratio along the substrate, which affects the morphology of MoS<sub>2</sub>, on the basic principle of crystal growth.<sup>18</sup> As we increase the amount of MoO<sub>3</sub> to 15 mg, the density of MoO<sub>3-x</sub> clusters increases gradually with a proper ratio 1:60 of Mo/S atom concentration, which forms a continuous film of MoS<sub>2</sub> flakes. Higher concentrations of MoO<sub>3</sub> lead to multiple MoS<sub>2-x</sub> clusters resulting in the formation of multilayer growth. 30 mg MoO<sub>3</sub> precursor leads to the formation of multiple bright spots due to incomplete sulfurization of a number of clusters.<sup>22,23</sup> With increasing MoO<sub>3</sub> weight fraction, the coverage area monotonically increases, while the variation in domain size shows a maximum at 15 mg of MoO<sub>3</sub>, as shown graphically in Figure 4f (Figure S1—Supporting Information). Schematically shows the variation of the nucleation centers density with increasing MoO<sub>3</sub> concentration. This is in agreement with previous reports where 15 mg of MoO<sub>3</sub> was found to result in a continuous sheet of MoS<sub>2</sub>,<sup>18,21</sup> and the concentration of Mo governs the shape and size of monolayer MoS<sub>2</sub> crystals.<sup>40</sup>

To understand the change in the crystal structure and to quantify the number of layers, samples of SET-1 were subjected to Raman spectroscopy measurements. Spectra were collected from different regions of the sample, as shown in Figure 5a. Raman spectra shows two prominent

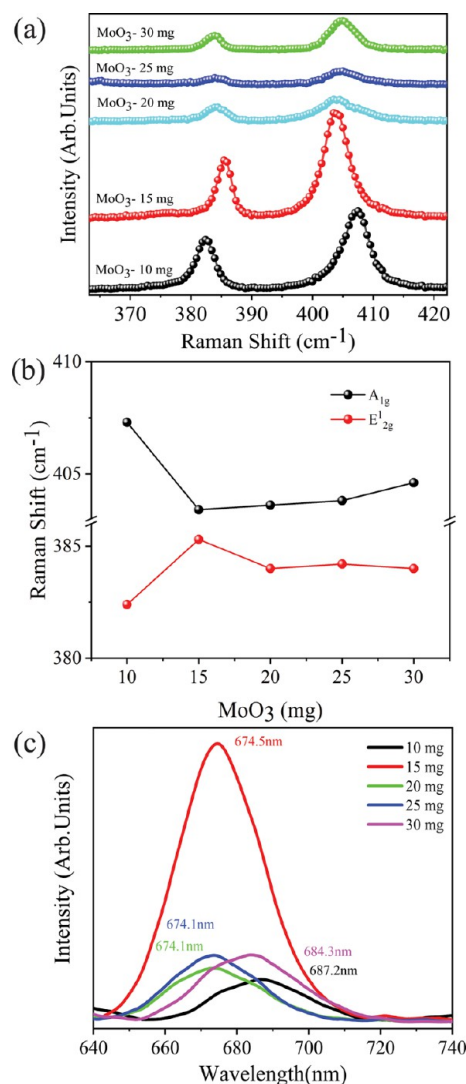


**Figure 5.** (a) Raman spectra of grown MoS<sub>2</sub> with varying MoO<sub>3</sub> weight fraction, (b) variation in the Raman shift position of A<sub>1g</sub> and E<sub>2g</sub>, and (c) photoluminescence spectra of MoS<sub>2</sub> grown by varying MoO<sub>3</sub> weight fraction.

peaks at  $\sim 383$  and  $\sim 404\ \text{cm}^{-1}$  assigned to the in-plane E<sub>2g</sub><sup>1</sup> vibration mode and out-of-plane A<sub>1g</sub> vibration mode. In-plane E<sub>2g</sub><sup>1</sup> vibration mode arises due to in-plane vibration of Mo and S atoms, while the out-of-plane A<sub>1g</sub> vibration mode arises due to out-of-plane vibration of sulfur atoms.<sup>33</sup> The peak width of these modes was estimated upon fitting E<sub>2g</sub><sup>1</sup> and A<sub>1g</sub> modes with Gaussian and Lorentzian line-shape, respectively (fitted curves Figure S2 and summarized Table S1 shown in the Supporting Information). Lorentzian line shape indicates high crystallinity of as-grown MoS<sub>2</sub> films. The difference in the peak position of E<sub>2g</sub><sup>1</sup> and A<sub>1g</sub> modes indicates the number of layers due to weak van der Waals interlayer coupling, and the presence of coulombic interlayer interactions in MoS<sub>2</sub>.<sup>33</sup> E<sub>2g</sub><sup>1</sup> and A<sub>1g</sub> modes are shifted as additional layers added to form the bulk material from individual layers because the interlayer van der Waals interaction increase the effective restoring force acting on the atoms.<sup>41</sup> With decreasing number of layers, A<sub>1g</sub> mode shifts closer to E<sub>2g</sub><sup>1</sup> modes.<sup>33</sup> The sample grown with 10, 15, 20, 25, and 30 mg shows peak separation of 24.9, 18.1, 19.6, again 19.6, and 20.6 cm<sup>-1</sup>, respectively. Raman spectra of 10 mg MoO<sub>3</sub> grown samples shows the multilayer growth



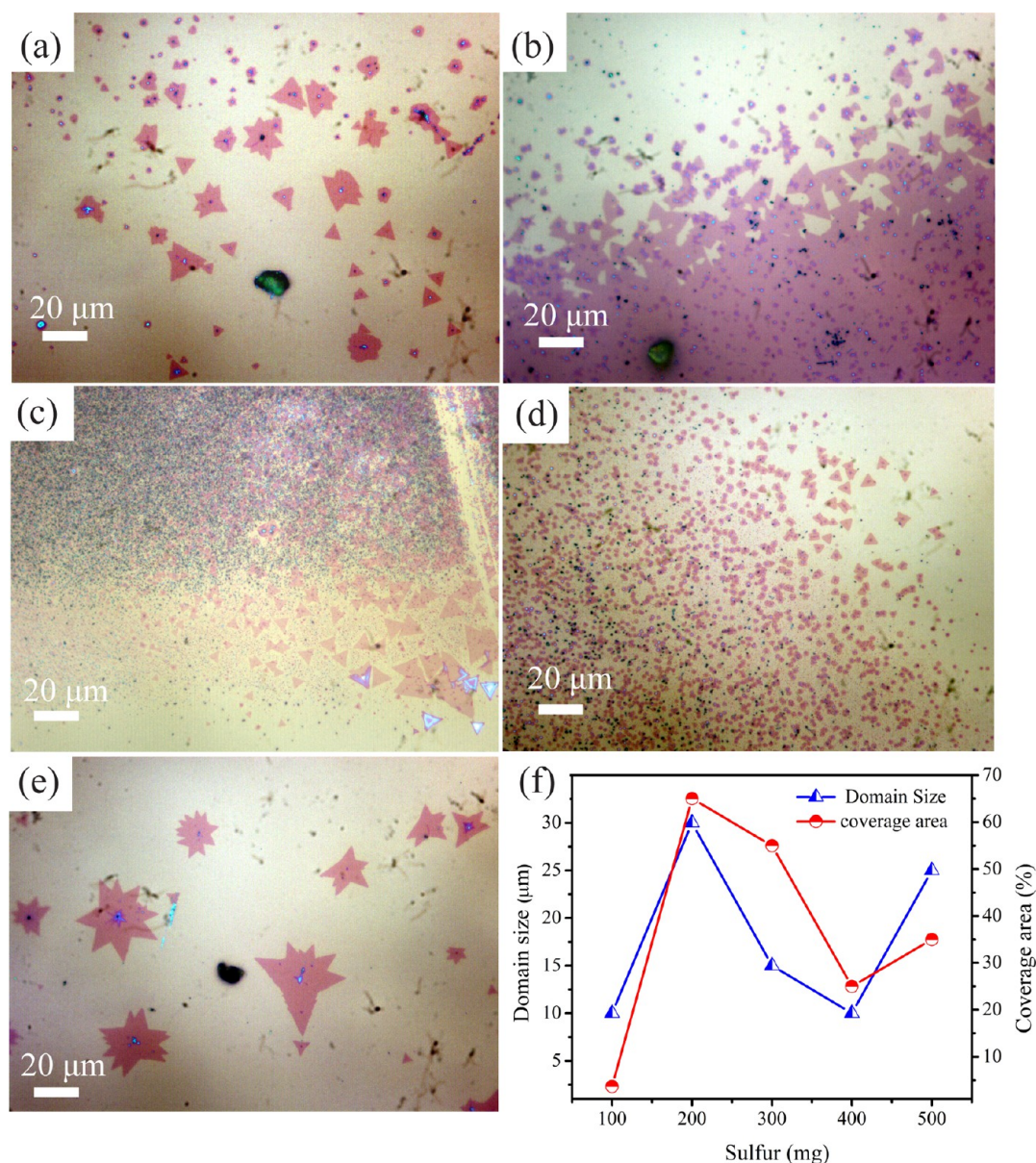


**Figure 6.** Optical microscopy images for the CVD-grown MoS<sub>2</sub> flakes with varying amounts of sulfur (a) 100, (b) 200, (c) 300, (d) 400, (e) 500 mg, and (f) dependence of domain size and coverage area on the weight fraction of the sulfur.

formation, while with 15, 20, and 25 mg of MoO<sub>3</sub> indicated monolayer growth. While growth with 30 mg of MoO<sub>3</sub> indicates bilayer growth. The higher relative concentration of MoO<sub>3</sub> as compared to sulfur leads to initialization of multi-nucleation sites resulting in multilayer growth, while growth with 15, 20, and 25 mg of MoO<sub>3</sub> results in monolayered growth. In the case of layered growth, the deposited MoO<sub>3</sub> “wets” the substrate due to dominance of surface tension between substrate-vapor ( $\gamma_{sv}$ ) over the combined effect of surface tension between film-substrate ( $\gamma_{fs}$ ) and film-vapor ( $\gamma_{fv}$ ), that is,  $\gamma_{sv} \geq \gamma_{fs} + \gamma_{fv}$ .<sup>38</sup> Figure 5b shows the peak position ( $E_{2g}^1$  and  $A_{1g}$ ) of Raman shift affected by the MoO<sub>3</sub> concentration. We observed, at lower concentrations of MoO<sub>3</sub> (10 mg), the peak difference is larger, as we increase the MoO<sub>3</sub> concentration (15 mg) keeping other precursors constant, the mode comes closer and their difference remarkably diminishes. However, as we increase the amount of MoO<sub>3</sub> (20 and 25 mg), there is a slight change in the  $E_{2g}^1$

mode w.r.t 15 mg of MoO<sub>3</sub> and no significant change is observed in the  $A_{1g}$  mode. In case of 30 mg MoO<sub>3</sub> precursor, both the modes are significantly shifted away from each other indicating the increase in number of layer of growth. Figure 5c shows photoluminescence spectra of samples. The grown sample with 10 mg of MoO<sub>3</sub> shows peaks at ~686.6 nm (1.80 eV). MoO<sub>3</sub>-10 shows a relatively weaker luminescence peak, indicating multilayer growth in agreement with observed Raman spectra. With the increase of MoO<sub>3</sub> weight fraction to 15 mg and higher, that is, 20 and 25 mg, the emission peak shifts to ~674.1 nm (1.84 eV) with varying intensities. Growth using 15 mg of MoO<sub>3</sub> shows the strongest emission intensity and with further increase of MoO<sub>3</sub> weight fraction, the PL intensity monotonically decreases. A strong emission indicates the presence of a direct band and high crystalline quality of grown monolayer films, when 15 mg of MoO<sub>3</sub> is used. At 30 mg, it shifts to ~684.6 nm (1.81 eV) indicating the increasing number of layers to 2, that is, bilayer with suppressed

intensity.<sup>5</sup> At lower concentrations (10 mg) and moderate 15 mg concentration of  $\text{MoO}_3$ , we observed a planar flake but with a higher concentration (20 and 25 mg) the flakes contended with nanocrystals on  $\text{MoS}_2$  flakes. At much higher concentrations (30 mg), the size decreased with the increase in the density of nanocrystals over the  $\text{MoS}_2$  flakes. Thus, the concentration of  $\text{MoO}_3$  is responsible for the self-seeding process and their concentration decides the nucleation site and coverage area. At much higher concentrations, the density of nanocrystals increases indicating incomplete sulfurization. Similar observations have been reported by Zhu et al.<sup>22</sup>

Figure 6 shows the growth of  $\text{MoS}_2$  with varying amounts of sulfur relative to  $\text{MoO}_3$  (SET-II), keeping weight of the  $\text{MoO}_3$  powder fixed at 15 mg and gas flow rate 100 sccm. Figure 6a shows results with 100 mg of sulfur.  $\text{MoS}_2$  flakes at random locations on the substrate were formed having shapes varying from triangle to star-like patterns with a crystallite size of  $\sim 11 \mu\text{m}$ . There is a small triangular growth of  $\text{MoS}_2$  flakes on the substrate due to lower concentrations of sulfur in the growth atmosphere near the surface. Doubling the sulfur amount to 200 mg results in a crystallite size of  $\sim 30 \mu\text{m}$  and continuous film upto few  $\text{mm}^2$ , as observed in Figure 6b. With further increase of weight fraction to 300 mg of sulfur,  $\text{MoS}_2$  crystals with a triangular shape and varying crystallite sizes  $\sim 7$  to  $25 \mu\text{m}$  were observed, as shown in Figure 6c. Also, crystallite domains were not continuous as observed at lower weight fractions. If the weight of the sulfur is increased to 400 mg, the crystallite size of the triangular  $\text{MoS}_2$  flakes is reduced to  $\sim 7 \mu\text{m}$  due to a decrease in the lower concentration of an Mo/S atom ratio, as shown in Figure 6d. With excessively large weight fractions of sulfur to 500 mg, the formation of star-like flakes were observed having an average crystallite size of about  $\sim 20 \mu\text{m}$  (Figure 6e). A closer observation to the center of the star flakes indicates the presence of clusters responsible for multi-nucleation. Due to the sufficient amount of sulfur, multilayer formation is observed. A proper weight fraction of sulfur has been observed as the prime factor deciding the formation of a number of layers/crystallite size. It is clear from optical micrographs that a proper amount of Mo/S ratio of the precursor plays a critical role in maintaining the triangular shape.<sup>42</sup> With varying concentrations of sulfur, the nucleation density significantly changes in contrast to previous reports, where the role of sulfur in nucleation was found to be negligible.<sup>20</sup>

Figure 7a shows Raman spectra of samples grown using varying sulfur weight fraction in the range 100–500 mg. The peak was estimated upon fitting  $E_{2g}^1$  and  $A_{1g}$  modes with Gaussian and Lorentzian line-shapes, respectively (fitted curves Figure S3 and summarized Table S2 shown in the Supporting Information). While with lower concentrations of sulfur (100 mg), the peak position difference is  $\sim 23.2 \text{ cm}^{-1}$ , which indicates the formation of more than one layer. However, further increase of amount of sulfur (200 mg) results in the peak difference lowering to  $\sim 18.2 \text{ cm}^{-1}$ , indicating the growth of monolayers with high crystallinity. As we increase the amount of sulfur (to 300 mg), the peak difference increases to  $\sim 20.0 \text{ cm}^{-1}$  indicating the formation of monolayers. While with further increase in the amount of sulfur (to 400 and 500 mg), the peak difference sequentially increases to  $\sim 24.1$  and  $25.1 \text{ cm}^{-1}$  which indicates multilayer formation. Figure 7b clearly shows a correlation between the amount of sulfur and the  $E_{2g}^1$  and  $A_{1g}$  Raman peak position. It indicates both the in-plane and out-of-plane modes are shifted with the amount of

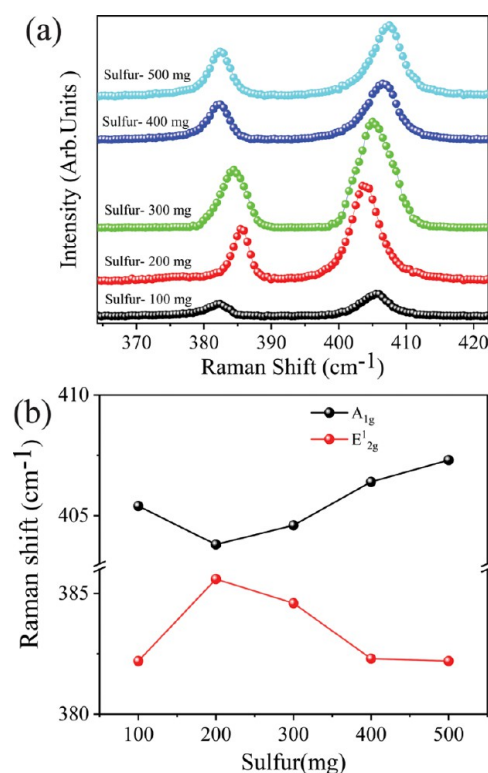


**Figure 7.** (a) Raman spectra of grown  $\text{MoS}_2$  with varying sulfur weight fraction and (b) variation in the Raman shift position of  $A_{1g}$  and  $E_{2g}^1$ .

sulfur. Sulfur is found to play an important role in controlling the number of layers and a proper concentration of sulfur with respect to the  $\text{MoO}_3$  precursor and gas flow rate favors monolayer growth. Sulfur helps to increase the vertical growth, as shown in Figure 6 and the coverage area decreases with higher amount of sulfur. We obtain a star-like shape with multilayer growth with increased sulfur content. This is in agreement with Raman spectra. The shift in the Raman peak with varying amounts of sulfur is shown in Figure 7b. The graph shows that with amount of sulfur both the in plane or out of plane are shifted far apart, demonstrating the increase in the number of layers due to the amount of sulfur.

Figure 8 shows optical micrographs of  $\text{MoS}_2$  samples grown with varying gas flow rates (50–300 sccm) keeping precursor weights of  $\text{MoO}_3$  (15 mg) and sulfur (200 mg) constant. Growth with 50 sccm of argon flow results in  $\text{MoS}_2$  flakes having a large crystallite size of  $\sim 80 \mu\text{m}$  and coverage area of  $\sim 40\%$ , as shown in Figure 8a. With moderate gas flow rates (100 and 150 sccm), the discrete crystals of  $\text{MoS}_2$  flakes join together to form continuous films. A gas flow rate of 100 sccm results in a coverage area of 70% estimated using ImageJ software, while a flow rate of 150 sccm leads to 92% coverage area, as shown in Figure 8b. Further increases of gas flow rate to 200, 250, and 300 sccm result in smaller crystallites with discrete regions. A gas flow rate of 300 sccm results in  $\text{MoS}_2$  crystallites of size as small as  $\sim 7 \mu\text{m}$ . It is obvious from the optical micrographs shown in Figure 8c–e, respectively, that carrier gas flow rates are another key parameter which influence the crystallite size and coverage area by tuning the local concentration of  $\text{MoO}_{3-x}$  and sulfur vapor precursors being nucleated on the substrate. Carrier gas flow rate decides the residence time of vapors of precursors on the substrate



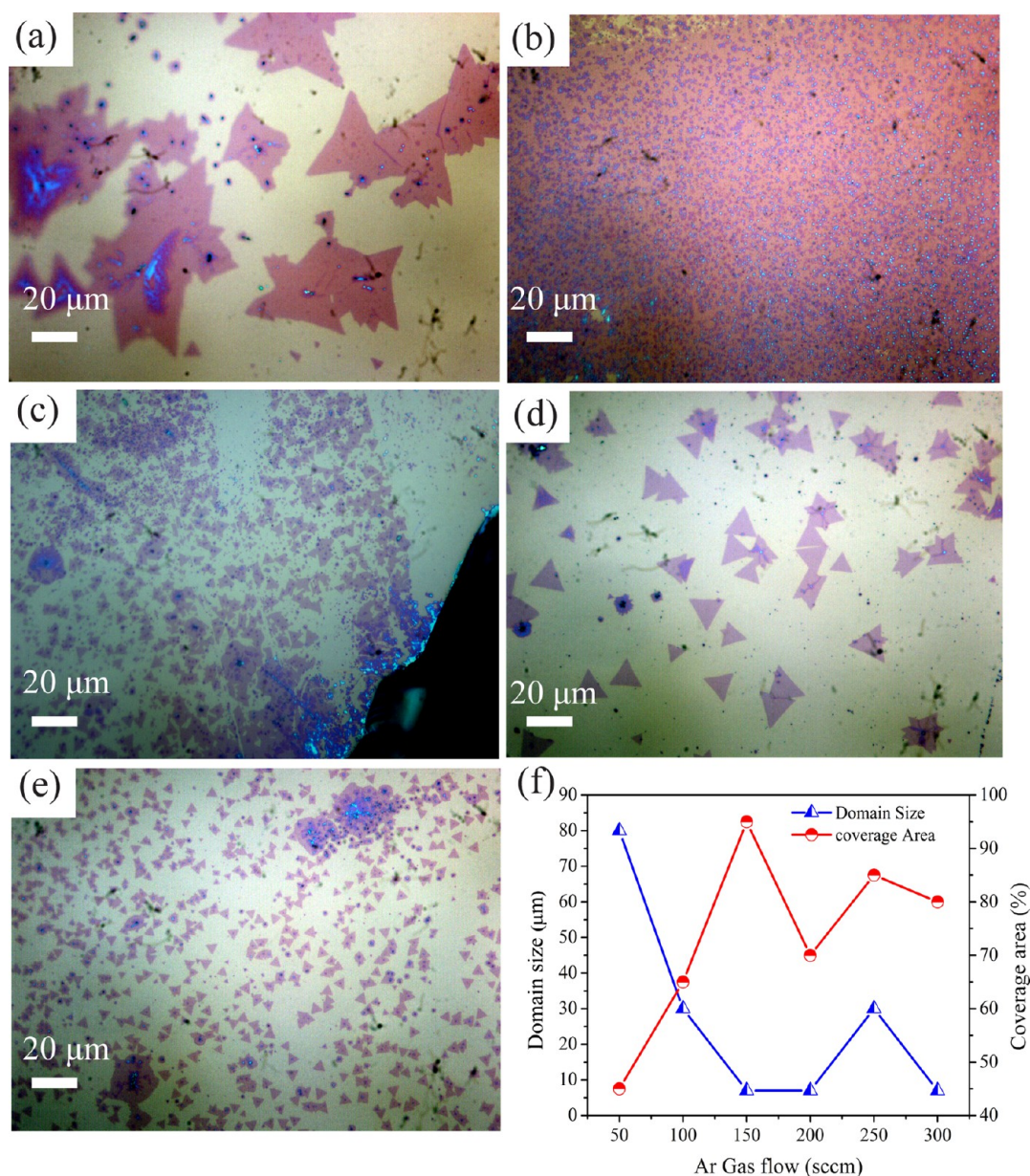


**Figure 8.** Optical image for CVD grown MoS<sub>2</sub> flakes with varying gas flow rates (a) 50, (b) 150, (c) 200, (d) 250, (e) 300 sccm, and (f) dependence of coverage area and crystallite size on the carrier gas flow rate.

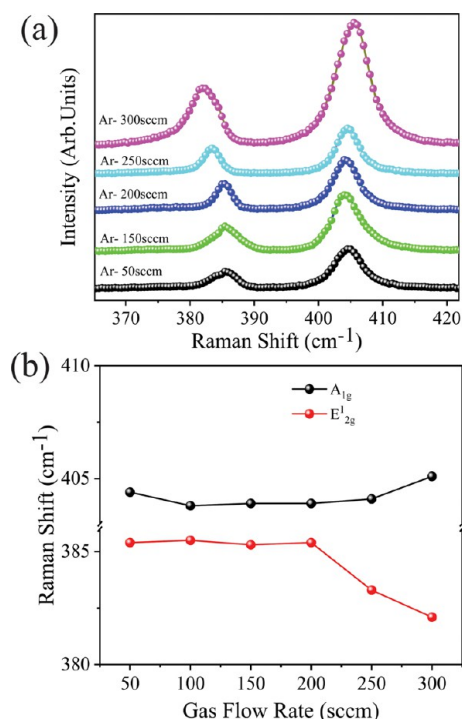
deciding nucleation density, crystallite size, and coverage area. Under sufficient supply of precursors and nucleation sites, the growth extends in the form of a large-area single-layered MoS<sub>2</sub> continuous film with increasing gas flow rate, as shown in Figure 8f. It is also interesting to note that with the increase of the crystallite size, the coverage area decreases.

Raman spectra of gas flow variation are shown in Figure 9a, it explains the role of gas flow rate in terms of vertical growth of layer by keeping the amount of both the precursors fixed. All these peaks were estimated upon fitting  $E_{2g}^1$  and  $A_{1g}$  modes with Gaussian and Lorentzian line-shapes, respectively (fitted curves Figure S3 and summarized in Table S3 shown in the Supporting Information). The Raman peak difference between two modes for lower and moderate gas flow rates (50, 100, and 150 sccm) are  $\sim 19.0$ ,  $18.2$ , and  $18.6$   $\text{cm}^{-1}$  observed sequentially. This difference is a clear indication of formation of monolayer MoS<sub>2</sub>. With high gas flow rates (200 sccm), the difference remains the same  $\sim 18.5$   $\text{cm}^{-1}$ ; but at 250 and 300

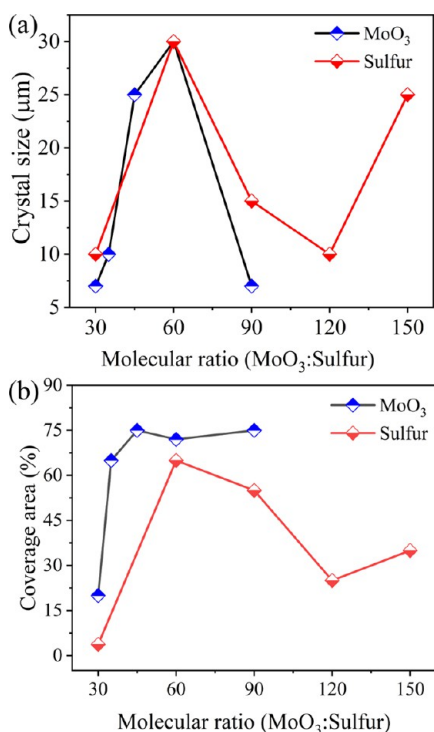
sccm, the Raman shift difference increases to  $\sim 20.8$  and  $23.0$   $\text{cm}^{-1}$  representing the bilayer and multilayer growth. Figure 9b shows the Raman peak position with different gas flow rates. As we increase the gas flow rate from lower (50 sccm) to higher (200 sccm), the  $E_{2g}^1$  does not show a significant change, but for much higher gas flow rates (250 and 300 sccm) a significant change is observed. A closer look at the  $A_{1g}$  mode, a slight change is observed when the gas flow rate is changed from 50 to 200 sccm, while at higher gas flow rates (250 and 300 sccm), the change is easily noticed indicating growth of bilayer to multilayer growth.

Figure 10a,b shows the effect of change of molar ratio of Mo and sulfur on the crystallite size and on the coverage area. With variation of gas flow rate, the atomic ratio of precursors (i.e., Mo/S) near the SiO<sub>2</sub>/Si substrate changes and it is found to be responsible for the change in the morphology observed. With increasing molar ratio from 30:1 to 60:1, the crystallite size increases. With further increase of the molar ratio, the





**Figure 9.** (a) Raman spectra of grown MoS<sub>2</sub> with varying MoO<sub>3</sub> weight fraction and (b) variation in the Raman shift position of A<sub>1g</sub> and E<sub>2g</sub>.



**Figure 10.** Effect of molecular ratio (MoO<sub>3</sub>/sulfur) on the (a) crystallite size and (b) coverage area %.

crystallite size monotonically decreases for molar ratios 90:1 and 120:1. Growth using increased molar ratio to 150:1 shows an increase in the crystallite size. A molar ratio of 60:1 results in the continuous film with a MoS<sub>2</sub> average crystallite size of ~30 μm. MoS<sub>2</sub> crystals grown with a molar ratio of 60:1 show the highest photoluminescence intensity indicating monolayer

growth. Under all attempted growth conditions by varying precursor's weight fractions and gas flow rates, we obtained triangular shaped MoS<sub>2</sub> growth. While Senithikumar et al.<sup>43</sup> observed variations in the grown crystallite shape from growth under low pressure conditions. It is interesting to observe that the crystallite shape remains triangular for growth under atmospheric pressure conditions using a single zone furnace without any requirement of vacuum conditions.

## 5. CONCLUSIONS

Through controlled growth at various experimental parameters, we have been able to successfully grow continuous films of MoS<sub>2</sub> monolayers on the SiO<sub>2</sub>/Si substrate through CVD. Optimized precursor weight ratio, that is, MoO<sub>3</sub> and sulfur (15 mg:200 mg) results in discrete crystallite size as large as 80 μm with 50 sccm flow of argon as a carrier gas and coverage area of ~40%. Thus, the concentration of MoO<sub>3</sub> is responsible for the self-seeding process and their concentration decides the nucleation site and coverage area. With moderate gas flow rates (100 and 150 sccm), the discrete crystals of MoS<sub>2</sub> flakes join together to form continuous films. A gas flow rate of 100 sccm results in a continuous film with 70% coverage area. While a flow rate of 150 sccm leads to 92% coverage area and increase of the crystallite size with decreased coverage area. MoO<sub>3-x</sub> was found to be responsible for self-seeding nucleation and its amount decides the nucleation density. The formation of MoS<sub>2</sub> flakes and their shape is dependent on the local concentration, which is tuned by the relative amount of MoO<sub>3</sub> and sulfur precursors. The carrier gas flux decides the residence time of Mo and S on the substrate toward growth. The carrier gas flow rate is responsible for local concentration of vapor precursors and their coverage area.

## ■ ASSOCIATED CONTENT

### Supporting Information

The Supporting Information is available free of charge at <https://pubs.acs.org/doi/10.1021/acsomega.2c07408>.

Growth mechanism schematic and Raman spectra of samples with fitted peak along with summary of line profile parameters (PDF)

## ■ AUTHOR INFORMATION

### Corresponding Author

Dilip K. Singh – Department of Physics, Birla Institute of Technology Mesra, Ranchi 835215, India; [orcid.org/0000-0002-8162-7766](https://orcid.org/0000-0002-8162-7766); Email: [dilipsinghnano1@gmail.com](mailto:dilipsinghnano1@gmail.com)

### Author

Rakesh K. Prasad – Department of Physics, Birla Institute of Technology Mesra, Ranchi 835215, India

Complete contact information is available at:

<https://pubs.acs.org/doi/10.1021/acsomega.2c07408>

### Author Contributions

The manuscript was written through contributions of both authors. All authors have given approval to the final version of the manuscript.

### Notes

The authors declare no competing financial interest.

## ACKNOWLEDGMENTS

Dilip K. Singh thanks UGC-DAE CSR Indore (CRS/2021-22/01/358), NM-ICPS ISI Kolkata, and DST, Government of India (CRG/2021/002179; CRG/2021/003705) for financial support.

## REFERENCES

- (1) Radisavljevic, B.; Radenovic, A.; Brivio, J.; Giacometti, V.; Kis, A. Single-layer MoS<sub>2</sub> transistors. *Nat. Nanotechnol.* **2011**, *6*, 147.
- (2) Wang, Q. H.; Kalantar-Zadeh, K.; Kis, A.; Coleman, J. N.; Strano, M. S. Electronics and optoelectronics of two-dimensional transition metal dichalcogenides. *Nat. Nanotechnol.* **2012**, *7*, 699–712.
- (3) Balendhran, S.; Walia, S.; Nili, H.; Ou, J. Z.; Zhuiykov, S.; Kaner, R. B.; Sriram, S.; Bhaskaran, M.; Kalantar-zadeh, K. Two-dimensional molybdenum trioxide and dichalcogenides. *Adv. Funct. Mater.* **2013**, *23*, 3952–3970.
- (4) Mak, K. F.; Lee, C.; Hone, J.; Shan, J.; Heinz, T. F. Atomically thin MoS<sub>2</sub>: a new direct-gap semiconductor. *Phys. Rev. Lett.* **2010**, *105*, 136805.
- (5) Splendiani, A.; Sun, L.; Zhang, Y.; Li, T.; Kim, J.; Chim, C.-Y.; Galli, G.; Wang, F. Emerging photoluminescence in monolayer MoS<sub>2</sub>. *Nano Lett.* **2010**, *10*, 1271–1275.
- (6) Novoselov, K. S.; Jiang, D.; Schedin, F.; Booth, T.; Khotkevich, V.; Morozov, S.; Geim, A. K. Two-dimensional atomic crystals. *Proc. Natl. Acad. Sci.* **2005**, *102*, 10451–10453.
- (7) Coleman, J. N.; Lotya, M.; O'Neill, A.; Bergin, S. D.; King, P. J.; Khan, U.; Young, K.; Gaucher, A.; De, S.; Smith, R. J.; Shvets, I. V.; Arora, S. K.; Stanton, G.; Kim, H.-Y.; Lee, K.; Kim, G. T.; Duesberg, G. S.; Hallam, T.; Boland, J. J.; Wang, J. J.; Donegan, J. F.; Grunlan, J. C.; Moriarty, G.; Shmeliov, A.; Nicholls, R. J.; Perkins, J. M.; Grievson, E. M.; Theuwissen, K.; McComb, D. W.; Nellist, P. D.; Nicolosi, V. Two-dimensional nanosheets produced by liquid exfoliation of layered materials. *Science* **2011**, *331*, 568–571.
- (8) Zeng, Z.; Yin, Z.; Huang, X.; Li, H.; He, Q.; Lu, G.; Boey, F.; Zhang, H. Single-layer semiconducting nanosheets: high-yield preparation and device fabrication. *Angew. Chem.* **2011**, *123*, 11289–11293.
- (9) Liu, K.-K.; Zhang, W.; Lee, Y.-H.; Lin, Y.-C.; Chang, M.-T.; Su, C.-Y.; Chang, C.-S.; Li, H.; Shi, Y.; Zhang, H.; Lai, C.-S.; Li, L.-J. Growth of large-area and highly crystalline MoS<sub>2</sub> thin layers on insulating substrates. *Nano Lett.* **2012**, *12*, 1538–1544.
- (10) Gong, C.; Huang, C.; Miller, J.; Cheng, L.; Hao, Y.; Cobden, D.; Kim, J.; Ruoff, R. S.; Wallace, R. M.; Cho, K.; Xu, X.; Chabal, Y. J. Metal contacts on physical vapor deposited monolayer MoS<sub>2</sub>. *ACS Nano* **2013**, *7*, 11350–11357.
- (11) Tan, L. K.; Liu, B.; Teng, J. H.; Guo, S.; Low, H. Y.; Loh, K. P. Atomic layer deposition of a MoS<sub>2</sub> film. *Nanoscale* **2014**, *6*, 10584–10588.
- (12) Jin, Z.; Shin, S.; Kwon, S.-J.; Han, Y.-S.; Min, Y.-S. Novel chemical route for atomic layer deposition of MoS<sub>2</sub> thin film on SiO<sub>2</sub>/Si substrate. *Nanoscale* **2014**, *6*, 14453–14458.
- (13) Rao, C.; Nag, A. Inorganic analogues of graphene. *Eur. J. Inorg. Chem.* **2010**, *2010*, 4244–4250.
- (14) Zhan, Y.; Liu, Z.; Najmaei, S.; Ajayan, P. M.; Lou, J. Large-area vapor-phase growth and characterization of MoS<sub>2</sub> atomic layers on a SiO<sub>2</sub> substrate. *Small* **2012**, *8*, 966–971.
- (15) Lee, Y.; Lee, J.; Bark, H.; Oh, I.-K.; Ryu, G. H.; Lee, Z.; Kim, H.; Cho, J. H.; Ahn, J.-H.; Lee, C. Synthesis of wafer-scale uniform molybdenum disulfide films with control over the layer number using a gas phase sulfur precursor. *Nanoscale* **2014**, *6*, 2821–2826.
- (16) Choudhary, N.; Park, J.; Hwang, J. Y.; Choi, W. Growth of large-scale and thickness-modulated MoS<sub>2</sub> nanosheets. *ACS Appl. Mater. Interfaces* **2014**, *6*, 21215–21222.
- (17) Lin, Y.-C.; Zhang, W.; Huang, J.-K.; Liu, K.-K.; Lee, Y.-H.; Liang, C.-T.; Chu, C.-W.; Li, L.-J. Wafer-scale MoS<sub>2</sub> thin layers prepared by MoO<sub>3</sub> sulfurization. *Nanoscale* **2012**, *4*, 6637–6641.
- (18) Wang, S.; Rong, Y.; Fan, Y.; Pacios, M.; Bhaskaran, H.; He, K.; Warner, J. H. Shape evolution of monolayer MoS<sub>2</sub> crystals grown by chemical vapor deposition. *Chem. Mater.* **2014**, *26*, 6371–6379.
- (19) Ganorkar, S.; Kim, J.; Kim, Y.-H.; Kim, S.-I. Effect of precursor on growth and morphology of MoS<sub>2</sub> monolayer and multilayer. *J. Phys. Chem. Solids* **2015**, *87*, 32–37.
- (20) Lin, Z.; Zhao, Y.; Zhou, C.; Zhong, R.; Wang, X.; Tsang, Y. H.; Chai, Y. Controllable growth of large-size crystalline MoS<sub>2</sub> and resist-free transfer assisted with a Cu thin film. *Sci. Rep.* **2015**, *5*, 18596.
- (21) Mohapatra, P.; Deb, S.; Singh, B.; Vasa, P.; Dhar, S. Strictly monolayer large continuous MoS<sub>2</sub> films on diverse substrates and their luminescence properties. *Appl. Phys. Lett.* **2016**, *108*, 042101.
- (22) Zhu, D.; Shu, H.; Jiang, F.; Lv, D.; Asokan, V.; Omar, O.; Yuan, J.; Zhang, Z.; Jin, C. Capture the growth kinetics of CVD growth of two-dimensional MoS<sub>2</sub>. *npj 2D Mater. Appl.* **2017**, *1*, 8.
- (23) Zhou, D.; Shu, H.; Hu, C.; Jiang, L.; Liang, P.; Chen, X. Unveiling the growth mechanism of MoS<sub>2</sub> with chemical vapor deposition: from two-dimensional planar nucleation to self-seeding nucleation. *Cryst. Growth Des.* **2018**, *18*, 1012–1019.
- (24) Singh, A.; Moun, M.; Singh, R. Effect of different precursors on CVD growth of molybdenum disulfide. *J. Alloys Compd.* **2019**, *782*, 772–779.
- (25) Zhu, Z.; Zhan, S.; Zhang, J.; Jiang, G.; Yi, M.; Wen, J. Influence of growth temperature on MoS<sub>2</sub> synthesis by chemical vapor deposition. *Mater. Res. Express* **2019**, *6*, 095011.
- (26) Feng, S.; Tan, J.; Zhao, S.; Zhang, S.; Khan, U.; Tang, L.; Zou, X.; Lin, J.; Cheng, H. M.; Liu, B. Synthesis of Ultrahigh-Quality Monolayer Molybdenum Disulfide through In Situ Defect Healing with Thiol Molecules. *Small* **2020**, *16*, 2003357.
- (27) Ahn, C.; Park, Y.; Shin, S.; Ahn, J.-G.; Song, I.; An, Y.; Jung, J.; Kim, C. S.; Kim, J. H.; Bang, J.; Kim, D.; Baik, J.; Lim, H. Growth of Monolayer and Multilayer MoS<sub>2</sub> Films by Selection of Growth Mode: Two Pathways via Chemisorption and Physisorption of an Inorganic Molecular Precursor. *ACS Appl. Mater. Interfaces* **2021**, *13*, 6805–6812.
- (28) Zazyev, O. V.; Louie, S. G. Electronic transport in polycrystalline graphene. *Nat. Mater.* **2010**, *9*, 806–809.
- (29) Ganorkar, S.; Kim, J.; Kim, Y. H.; Kim, S.-I. Effect of Precursor on Growth of MoS<sub>2</sub> Monolayer and Multilayer. *J. Phys. Chem. Solid.* **2015**, *87*, 32.
- (30) Xie, Y.; Wang, Z.; Zhan, Y.; Zhang, P.; Wu, R.; Jiang, T.; Wu, S.; Wang, H.; Zhao, Y.; Nan, T.; Ma, X. Controllable growth of monolayer MoS<sub>2</sub> by chemical vapor deposition via close MoO<sub>2</sub> precursor for electrical and optical applications. *Nanotechnology* **2017**, *28*, 084001.
- (31) Tao, L.; Chen, K.; Chen, Z.; Chen, W.; Gui, X.; Chen, H.; Li, X.; Xu, J.-B. Centimeter-scale CVD growth of highly crystalline single-layer MoS<sub>2</sub> film with spatial homogeneity and the visualization of grain boundaries. *ACS Appl. Mater. Interfaces* **2017**, *9*, 12073–12081.
- (32) Han, G. H.; Kybert, N. J.; Naylor, C. H.; Lee, B. S.; Ping, J.; Park, J. H.; Kang, J.; Lee, S. Y.; Lee, Y. H.; Agarwal, R.; Johnson, A. Seeded growth of highly crystalline molybdenum disulfide monolayers at controlled locations. *Nat. Commun.* **2015**, *6*, 6128.
- (33) Lee, C.; Yan, H.; Brus, L. E.; Heinz, T. F.; Hone, J.; Ryu, S. Anomalous lattice vibrations of single- and few-layer MoS<sub>2</sub>. *ACS Nano* **2010**, *4*, 2695–2700.
- (34) Mignuzzi, S.; Pollard, A. J.; Bonini, N.; Brennan, B.; Gilmore, I. S.; Pimenta, M. A.; Richards, D.; Roy, D. Effect of disorder on Raman scattering of single-layer MoS<sub>2</sub>. *Phys. Rev. B: Condens. Matter Mater. Phys.* **2015**, *91*, 195411.
- (35) Coehoorn, R.; Haas, C.; De Groot, R. Electronic structure of MoSe<sub>2</sub>, MoS<sub>2</sub>, and WSe<sub>2</sub>. II. The nature of the optical band gaps. *Phys. Rev. B: Condens. Matter Mater. Phys.* **1987**, *35*, 6203.
- (36) Coehoorn, R.; Haas, C.; Dijkstra, J.; Flipse, C. d.; de Groot, R.; Wold, A. Electronic structure of MoSe<sub>2</sub>, MoS<sub>2</sub>, and WSe<sub>2</sub>. I. Band-structure calculations and photoelectron spectroscopy. *Phys. Rev. B: Condens. Matter Mater. Phys.* **1987**, *35*, 6195.
- (37) Dumcenco, D.; Ovchinnikov, D.; Marinov, K.; Lazić, P.; Gibertini, M.; Marzari, N.; Sanchez, O. L.; Kung, Y.-C.; Krasnozhan,



D.; Chen, M.-W.; Bertolazzi, S.; Gillet, P.; Fontcuberta i Morral, A.; Radenovic, A.; Kis, A. Large-area epitaxial monolayer MoS<sub>2</sub>. *ACS Nano* **2015**, *9*, 4611–4620.

(38) Ohring, M. *Materials Science of Thin Films*; Elsevier, 2001.

(39) Najmaei, S.; Liu, Z.; Zhou, W.; Zou, X.; Shi, G.; Lei, S.; Yakobson, B. I.; Idrobo, J.-C.; Ajayan, P. M.; Lou, J. Vapour phase growth and grain boundary structure of molybdenum disulphide atomic layers. *Nat. Mater.* **2013**, *12*, 754–759.

(40) Wang, W.; Zeng, X.; Wu, S.; Zeng, Y.; Hu, Y.; Ding, J.; Xu, S. Effect of Mo concentration on shape and size of monolayer MoS<sub>2</sub> crystals by chemical vapor deposition. *J. Phys. D: Appl. Phys.* **2017**, *50*, 395501.

(41) Molina-Sánchez, A.; Wirtz, L. Phonons in single-layer and few-layer MoS<sub>2</sub> and WS<sub>2</sub>. *Phys. Rev. B: Condens. Matter Mater. Phys.* **2011**, *84*, 155413.

(42) Withanage, S. S.; Khondaker, S. I. CVD Growth of Monolayer MoS<sub>2</sub> on Sapphire Substrates by using MoO<sub>3</sub> Thin Films as a Precursor for Co-Evaporation. *MRS Adv.* **2019**, *4*, 587–592.

(43) Senthilkumar, V.; Tam, L. C.; Kim, Y. S.; Sim, Y.; Seong, M.-J.; Jang, J. Direct vapor phase growth process and robust photoluminescence properties of large area MoS<sub>2</sub> layers. *Nano Res.* **2014**, *7*, 1759–1768.